Please cite this article in press as: Tummala et al., Inhibition of De Novo NAD+ Synthesis by Oncogenic URI Causes Liver Tumorigenesis through DNA Damage, Cancer Cell (2014), http://dx.doi.org/10.1016/j.ccell.2014.10.002

Cancer Cell
Article

Inhibition of De Novo NAD+ Synthesis by Oncogenic URI Causes Liver Tumorigenesis through DNA Damage

Krishna S. Tummala,[1] Ana L. Gomes,[1] Mahmut Yilmaz,[1] Osvaldo Graña,[2] Latifa Bakiri,[3] Isabel Ruppen,[4] Pilar Ximénez-Embún,[4] Vinayata Sheshappanavar,[5] Manuel Rodriguez-Justo,[6] David G. Pisano,[2] Erwin F. Wagner,[3] and Nabil Djouder[1,*]

[1]Growth Factors, Nutrients and Cancer Group, BBVA Foundation-Cancer Cell Biology Programme, Spanish National Cancer Research Centre, CNIO, 28029 Madrid, Spain
[2]Bioinformatics Unit, Structural Biology and Biocomputing Programme, Spanish National Cancer Research Centre, CNIO, 28029 Madrid, Spain
[3]Genes, Development, and Disease Group, BBVA Foundation-Cancer Cell Biology Programme, Spanish National Cancer Research Centre, CNIO, 28029 Madrid, Spain
[4]Proteomics Core Unit, ProteoRed ISCIII, Biotechnology Programme, Spanish National Cancer Research Centre, CNIO, 28029 Madrid, Spain
[5]Department of Pathology, Royal London Hospital, London E1 1BB, UK
[6]Department of Cellular Pathology, University College London NHS Trust, London NW1 2BU, UK
*Correspondence: ndjouder@cnio.es
http://dx.doi.org/10.1016/j.ccell.2014.10.002

SUMMARY

Molecular mechanisms responsible for hepatocellular carcinoma (HCC) remain largely unknown. Using genetically engineered mouse models, we show that hepatocyte-specific expression of unconventional prefoldin RPB5 interactor (URI) leads to a multistep process of HCC development, whereas its genetic reduction in hepatocytes protects against diethylnitrosamine (DEN)-induced HCC. URI inhibits aryl hydrocarbon (AhR)- and estrogen receptor (ER)-mediated transcription of enzymes implicated in L-tryptophan/kynurenine/nicotinamide adenine dinucleotide (NAD^+) metabolism, thereby causing DNA damage at early stages of tumorigenesis. Restoring NAD^+ pools with nicotinamide riboside (NR) prevents DNA damage and tumor formation. Consistently, URI expression in human HCC is associated with poor survival and correlates negatively with L-tryptophan catabolism pathway. Our results suggest that boosting NAD^+ can be prophylactic or therapeutic in HCC.

INTRODUCTION

Hepatocellular carcinoma (HCC) is the commonest, usually lethal, human primary liver neoplasm (GLOBOCAN v2.0, 2008). The early stage is characterized by low- to high-grade dysplastic nodules, "preneoplastic lesions" (Kudo, 2009). These frequently develop in chronic inflammatory liver disease or hepatitis, which can promote fibrosis, cirrhosis, and progression to HCC. Thus, precancerous lesions have clinical value for HCC prediction (Libbrecht et al., 2001), but therapeutic options are limited (El-Serag, 2011).

In early stages of many cancers, including HCC, oncogene activation induces replicative stress, resulting in DNA damage leading to chromosomal instability (CIN), which accelerates tumor development (Teoh et al., 2008). DNA damage elicits a key repair mechanism, the DNA damage response (DDR), initiated by phosphorylation of checkpoint proteins Chk1, Chk2, and p53 (Reinhardt and Schumacher, 2012). p53-dependent responses, including cell cycle arrest and/or senescence, are induced, limiting preneoplastic lesions' growth. When DNA damage is too pronounced, p53 engages an apoptotic program by

Significance

HCC is the third leading cause of cancer death worldwide with limited therapeutic options. Here we demonstrate that NAD^+ deficit-induced genotoxic stress is critical to initiate liver tumorigenesis and unravel a critical link between nutrient metabolism and genome integrity. Because our findings are relevant in human HCC, we propose that nutritional supplementation of NR, a vitamin B3 derivative, or other NAD^+ boosters can be used as preventive and curative therapies in oncogene-induced NAD^+ depletion-mediated DNA damage and carcinogenesis, especially in patients with precancerous lesions. Therapeutic intervention on metabolic alterations prior to genomic instability should be further considered to prevent tumorigenesis.

Please cite this article in press as: Tummala et al., Inhibition of De Novo NAD+ Synthesis by Oncogenic URI Causes Liver Tumorigenesis through DNA Damage, Cancer Cell (2014), http://dx.doi.org/10.1016/j.ccell.2014.10.002

upregulation of Bcl-2 family proteins (Noxa, Puma, Bid, and/or Bax). p53 dysfunctions allow tumor cells to escape apoptosis, and thus, mutations inactivating p53 are the most common alterations observed in HCC (Reinhardt and Schumacher, 2012).

In pathophysiological situations, the balance between cell proliferation and apoptosis can be altered, perturbing tissue homeostasis. Apoptotic dysregulations are important in liver disease. Insufficient apoptosis, eliminating mutated cells, combined with inflammation-mediated proliferation can promote liver cancer development. Excessive or sustained apoptosis causes liver injuries, increased hepatocyte regeneration, which enhances genetic errors and predisposes to HCC (Malhi and Gores, 2008). Still, the initiating hepatocarcinogenesis events remain unclear. Developing experimental models mimicking distinct stages of HCC development would help to explore molecular mechanisms linking histopathological changes to hepatocarcinogenesis.

Unconventional prefoldin RBP5 interactor (URI), a member of the R2TP/URI-prefoldin (PFD)-like complex containing the heat shock protein 90 (HSP90) (Boulon et al., 2010), is an oncogene amplified in human ovarian carcinomas and downstream effector of the growth factor and nutrient-regulated mTOR/S6K1 signaling cascade (Theurillat et al., 2011). URI inhibits phosphatase PP1γ, thereby increasing S6K1 activity-dependent survival signaling. Thus, URI/PP1γ complexes maintain the mitochondrial threshold for apoptosis in accordance to nutrient availability. URI overexpression promotes survival, while its deletion enhances cancer cell death (Djouder et al., 2007; Theurillat et al., 2011). Prompted by these observations, and the fact that HCC occurs on the basis of mitochondrial dysfunction-mediated hepatocyte death and liver injury (Luedde et al., 2014; Malhi and Gores, 2008), we investigate the role of URI in hepatocarcinogenesis.

RESULTS

URI Expression in Mouse Hepatocytes Induces Spontaneous Liver Tumors

We generated a *Col1a1* knockin mouse (Figures S1A and S1B available online), expressing human URI (hURI) via a tetracycline-dependent transactivator controlled by the hepatocyte-specific liver activated protein promoter (Figures S1C–S1E). These mice, designated hURI-tetOFF^{hep}, and littermates lacking hURI expression are referred to hereafter as "mutants" and "controls," respectively. Without doxycycline, hURI was expressed specifically in hepatocytes from one allele from E10.5 (Carpenter et al., 2005), roughly twice as much as mouse URI (Figures 1A, S1F, and S1G), similar to the increase of URI expression in human HCC (see below).

We observed no pathological signs in 3-week-old mutants. In 8-week-old mutants, hematoxylin and eosin (H&E) staining revealed anisokaryotic clusters (Figure 1B) resembling low-grade dysplastic nodules observed in human hepatitis (Libbrecht et al., 2001). At 12 weeks the clusters developed into high-grade dysplastic nodules (Figures 1B, S1H, and S1I), similar to human large liver cell dysplasia (LLCD) (Libbrecht et al., 2001). Fibrosis was detected at 8 weeks and increased over time until 24 weeks, as assessed by Sirius Red (SR), Masson Trichrome, alpha smooth muscle actin, type I collagen (COL1A1), and reticulin staining (Figure S1J). Quantification showed that about 1% to 3% of livers were SR positive in mutants, representing 100% to 300% increase over littermates (Figure S1K). Increases in fibrotic markers were measured by quantitative RT-PCR (Figures S1L–S1N), but serum alanine aminotransferase (ALT) values remained unchanged (Figure S1O).

Between 24–54 weeks macroscopic lesions including adenoma and early HCC emerged. Recent reports described malignant transformation of human adenomas, but tumors in our model developed simultaneously (Pilati et al., 2014). Between 54–65 weeks low-grade and differentiated HCC were fully apparent, and between 65–75 weeks, 40% of mutants developed macroscopic high-grade tumors occupying 20%–60% of the liver (Figures 1B, 1C, and S1P). There were 25%–50% of hepatocytes that were Ki67-positive, suggesting aggressive tumors (data not shown). According to World Health Organization criteria (WHO, 2008), all tumors were well/moderately differentiated: 20% glandular/acinar, indicative of telangiectatic variants, and 80% trabecular. No cholangiocarcinoma were detected (Figure 1C). Serum glucose, ALT, and total bile acids were affected (Figure S1Q). Surprisingly, serum albumin was increased, suggesting that liver function might not be fully compromised (Figure S1Q).

All mutants died at ~85 weeks, with a median survival of 76 weeks before complete liver failure (Figure 1D). Immunohistochemistry (IHC) and pathological analyses revealed hURI-positive hepatocyte-like cells in 30% of mutant lungs with HCC, indicating aggressive metastases (Figures S1R and S1S). Histopathological characterization confirmed the presence of heterogeneous tumors with collapsed reticulin fibers, suggesting increased hepatocyte death and proliferation, as indicated by Ki67 (Figure 1E). Increases in alpha fetoprotein (AFP) levels, a clinical marker for human HCC varied, but all tumors displayed dramatic increases in p53 abundance and phosphorylation (Figures 1E and 1F), suggesting that p53 may either carry mutations or may be improperly folded (Trinidad et al., 2013), thus possibly inactive.

Fully developed HCC appeared at 30 weeks in hepatocarcinogen diethylnitrosamine (DEN)-treated hURI-tetOFF^{hep} mice (Vesselinovitch and Mihailovich, 1983) (Figure S1T). When hURI was expressed from two alleles, increasing its expression to 6-fold compared to heterozygous hURI-tetOFF^{hep} mice, HCC were detected at 10 weeks (Figure S1U), highlighting the importance of URI dosage. Embryonic development was not involved because liver tumors were also detected in mice kept on doxycycline until 8 weeks (expressing hURI from 8 weeks) then transferred to normal (chow) diet (Figure S1V). Thus, hURI expression in mouse hepatocytes induces spontaneous HCC.

Continuous URI Expression Is Essential for Hepatocarcinogenesis

Ceasing hURI expression in 8-week-old mutants for 24 weeks reduced fibrosis and abolished dysplastic foci and prevented early tumors, without affecting liver-to-body weight ratios (Figures 2A–2D and S2A). S6K1 activity was increased in 24-week-old mice, but remained constant when hURI expression ceased, indicating that mTOR/S6K1 activation was hURI-independent (Figure 2B). Switching hURI expression off until 60 weeks prevented tumor development and normalized ALT levels (Figures S2B–S2E). Similarly, when hURI was expressed for 24 weeks,

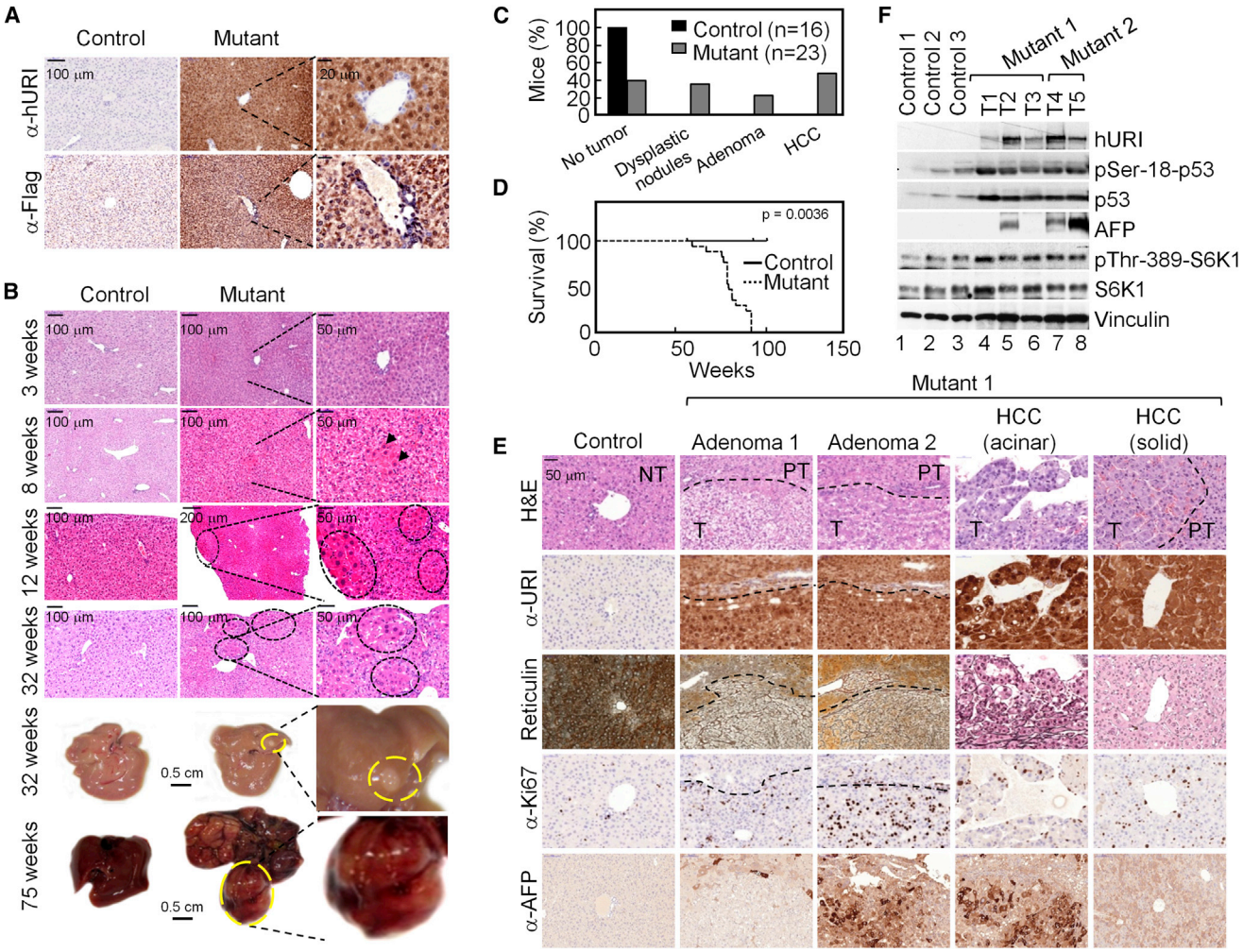

Figure 1. URI Expression in Mouse Hepatocytes Induces Spontaneous Liver Tumors

(A) Representative images of IHC stained liver sections from 3-week-old hURI-tetOFF^{hep} mice using hURI and FLAG antibodies. Insets represent the periportal area, showing hepatocyte specific hURI expression. (n > 10).

(B) Representative images of H&E stained liver sections from 3- (n > 6), 8- (n > 19), 12- (n > 11), and 32-week-old (n > 7) hURI-tetOFF^{hep} mice. Bottom two rows are representative images of whole livers from hURI-tetOFF^{hep} mice at 32 and 75 weeks of age. Black dotted circles mark LLCD-like lesions and black arrows point anisokaryotic clusters in mutant hURI-tetOFF^{hep} mice. Yellow dotted circles depict adenoma and HCC at 32 and 75 weeks of age, respectively.

(C) Percentage of control and mutant hURI-tetOFF^{hep} mice bearing liver abnormalities in 60- to 75-week-old-mice.

(D) Kaplan Meier curve of control (n = 17) and mutant (n = 17) hURI-tetOFF^{hep} mice. Log rank test p = 0.0036; Hazard ratio = 0.1603.

(E) Representative images of H&E, IHC, and reticulin stained liver sections from control and four tumors derived from one mutant hURI-tetOFF^{hep}. NT, PT, and T denote nontumoral, peritumoral, and tumoral tissues, respectively.

(F) WB analysis of control and mutant hURI-tetOFF^{hep} livers. "T" denotes tumor.

See also Figure S1.

until high-grade dysplastic nodules/early HCC and adenomas were apparent, then, switched-off for 28 weeks, only residual anisokaryotic clusters were detected, but no adenomas or HCCs (Figure 2E). However, ultrasound analysis demonstrated that well/moderately differentiated HCC (above 60 weeks) did not regress when hURI expression was ceased for 5 weeks (Figures S2F–S2H). Thus, continuous hURI expression is required for the maintenance of preneoplastic lesions and early tumors. Aggressive HCCs with sufficient genetic mutations become URI independent, even though ceasing URI expression for a longer time remains to be tested.

We genetically inactivated URI specifically in hepatocytes by crossing URI(lox/lox) and serum albumin (SA)-CreERT2 mice (Schuler et al., 2004). URI deletion in hepatocytes after tamoxifen treatment to obtain URI$^{(+/\Delta)hep}$ or URI$^{(\Delta/\Delta)hep}$ mice, was confirmed by IHC and western blotting (WB) (Figures 2F and 2G). Homozygous deletion of URI led to death of URI $^{(\Delta/\Delta)hep}$ mice around 10 days (Figure S2I). Disruption of tissue architecture, presence of atypia, dilated veins with intrahepatic bleeding, signs of necrosis, and inflammatory cell infiltration were observed by H&E staining. Additionally, SR staining, collapsed reticulin fibers, and increased ALT indicated that hepatocytes underwent

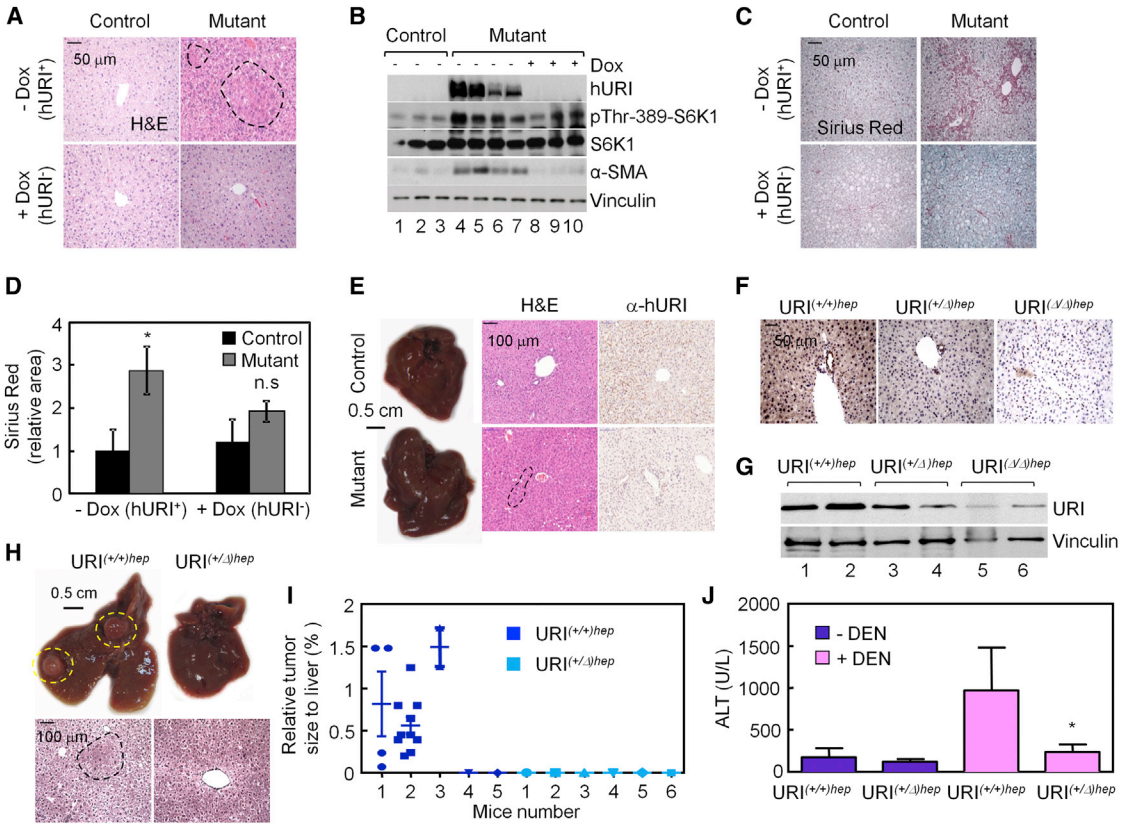

Figure 2. Continuous URI Expression Is Essential for Hepatocarcinogenesis

(A) Representative images of H&E stained liver sections from 32-week-old hURI-tetOFF^{hep} mice fed with (+) or without (−) doxycycline (Dox) after dysplatic lesion formation at 8 weeks. Dotted black circle represents premalignant lesions. (n ≥ 5).

(B) WB analysis of hURI-tetOFF^{hep} livers as described in (A).

(C) Representative images of Sirius Red stained liver sections from mice described in (A). (n ≥ 5).

(D) Quantification of Sirius Red stained liver sections from mice described in (C). (n ≥ 5).

(E) Representative images of full livers and H&E stained liver sections from hURI-tetOFF^{hep} mice treated with Dox for 28 weeks. Treatment started at 24 weeks of age, after the appearance of dysplastic lesions, adenomas, and early HCC. Dotted black circles denote reminiscent anisokaryotic areas. (n ≥ 5).

(F) Representative images of IHC stained liver sections for endogenous URI in URI$^{(+/+)hep}$, URI$^{(+/\Delta)hep}$, and URI$^{(\Delta/\Delta)hep}$ mice. (n ≥ 3).

(G) WB liver analysis for endogenous URI in URI$^{(+/+)hep}$, URI$^{(+/\Delta)hep}$, and URI$^{(\Delta/\Delta)hep}$ livers.

(H) Representative images of whole livers from URI$^{(+/+)hep}$ and URI$^{(+/\Delta)hep}$ mice treated with diethylnitrosamine (DEN) and sacrificed at 24 weeks of age. Dotted yellow circles depict liver tumors. (n ≥ 5). Bottom pictures represent reticulin stained livers, black circle depicts the dysplastic area.

(I) Tumor burden of mice described in (H).

(J) Serum ALT levels from mice described in (H).

Data represented as mean ± SEM (p ≤ 0.05 = *). See also Figure S2.

massive apoptotic program leading to liver injury, suggesting that these mice die from fulminant liver failure (Figures S2J and S2K). However, URI$^{(+/\Delta)hep}$ mice, in which URI expression was approximately halved (Figures 2F and 2G), supplied a liver damage-inducing 3,5-diethoxycarbonyl-1,4-dihydrocollidine (DDC)-supplemented diet, presented significantly less liver damage and fibrosis as shown by ALT, SR, and reticulin stainings (Figures S2L–S2N). Thus URI reduction protects from hepatocyte injury.

DEN-treatment increased URI levels in 3-week-old URI$^{(+/+)hep}$ mouse livers and in wild-type murine HCC (Figures S2O and S2P). Moreover, DEN induced tumor development at 24 weeks in 60% of URI$^{(+/+)hep}$ mice and enhanced ALT levels, but URI$^{(+/\Delta)hep}$ mice did not show any tumors at this age and displayed normal ALT values (Figures 2H–2J). Levels of cytochrome P450 2E1 and 1A1 catalyzing DEN were unchanged in 3-week-old livers of DEN-treated URI$^{(+/+)hep}$ and URI$^{(+/\Delta)hep}$ mice (Figure S2O), suggesting that halving URI levels does not affect DEN bioactivation (Kang et al., 2007). Thus, while complete deletion of URI induces liver injury, halving URI is beneficial to maintain liver homeostasis and prevents liver injury and HCC development.

URI-Induced DNA Damage Initiates Liver Tumorigenesis

To further elucidate the mechanisms of hepatocyte death and their contribution to HCC, we checked for phosphorylation of histone H2AX (γH2AX), a DNA damage marker that triggers apoptosis via the p53-DDR pathway. γH2AX and p53 phosphorylation and abundance did not differ in 1-week-old livers (Figure S3A). At 3 weeks, a nonpathological stage with no dysplastic lesions, γH2AX, phosphorylation of the 32 kDa subunit of replication protein A (RPA32) at Ser-4 and Ser-8, and p53 abundance

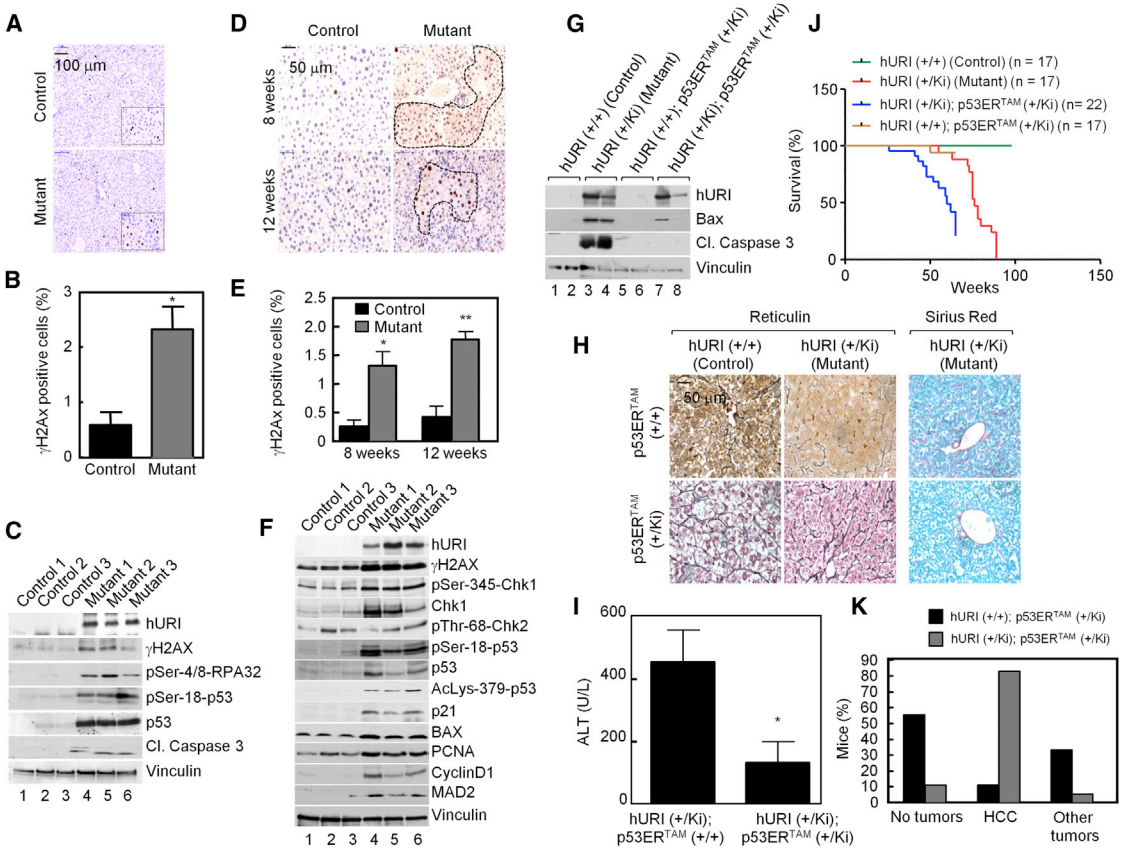

Figure 3. URI-Induced DNA Damage Initiates Liver Tumorigenesis

(A) Representative images of γH2AX IHC stained liver sections from 3-week-old hURI-tetOFF^{hep} mice. Insets denote γH2AX positive nuclei. (n = 5).

(B) Quantification of (A).

(C) WB analysis of 3-week-old hURI-tetOFF^{hep} livers.

(D) Representative images of γH2AX IHC stained liver sections from 8-week- and 12-week-old hURI-tetOFF^{hep} mice. Dotted black shapes depict anisokaryotic clusters positive for γH2AX. (n = 6).

(E) Quantification of (D).

(F) WB analysis of 8-week-old hURI-tetOFF^{hep} livers

(G) WB analysis of 8-week-old hURI-tetOFF^{hep} livers, with or without p53 inactivation.

(H) Reticulin and Sirius Red stained livers described in (G).

(I) Serum ALT levels of mutant mice with or without p53 inactivation. (n > 4).

(J) Kaplan-Meier survival curve of control and mutant hURI-tetOFF^{hep} mice with and without p53 inactivation. (Log rank test $p \leq 0.001$.)

(K) Percentage of tumor incidence in hURI-tetOFF^{hep} mice with or without p53 inactivation.

Data represented as mean ± SEM (*$p \leq 0.05$ and **$p \leq 0.01$). See also Figure S3.

and phosphorylation were higher in mutants (Figures 3A–3C), suggesting that DDR precedes precancerous lesions. While p53-dependent apoptosis occurred in cells that unsuccessfully repair DNA (cleaved caspase 3; Figure 3C), hepatocyte proliferation rate was reduced (Figures S3B and S3C), suggesting that high proliferation is not the initial hepatocarcinogenic event.

γH2AX-positive nuclei were more abundant in older mutant livers (8- to 12-week-old) with obvious dysplastic lesions. Furthermore, Ser-345 phosphorylation (and hence activation) of Chk1 was enhanced in mutants, but not Thr-68 phosphorylation of Chk2, suggesting single strand break (Reinhardt and Schumacher, 2012) (Figures 3D–3F). Enhanced p53 phosphorylation at Ser-18 (Chk1 target), acetylation at Ac-lys379 (Ito et al., 2001) (Figure 3F), and expression of p19ARF (Reinhardt and Schumacher, 2012) (Figure S3D) indicate p53 stabilization.

Senescence-associated β-galactosidase activity, expression of several p53 target genes, BAX, and p21 protein abundance were increased in 8- and 12-week-old mutants, while expression of *Xiap* was decreased (Figures 3F, S3E, and S3F) (Reinhardt and Schumacher, 2012), suggesting increased hepatocyte death as also shown by collapsed reticulin fibers (Figure S3G). Increased abundance of proliferating cell nuclear antigen, cyclin D1, and Ki67-positive nuclei suggested compensatory proliferation (Figures 3F and S3H). Finally, MAD2, a CIN marker and downstream effector of cyclin D1, was increased (Figure 3F). Thus, hURI expression in hepatocytes induces genotoxic stress, apoptosis, compensatory proliferation, and CIN.

To assess genotoxic stress-induced apoptosis in HCC development, p53 was inactivated in hURI-tetOFF^{hep} mice. In p53-inactivated 8-week-old mutants (hURI (+/Ki); p53ER^{TAM} (+/Ki)),

cleaved caspase 3, Bax expression, and collapsed fibers were decreased (Figures 3G and 3H). Furthermore, SR staining and ALT levels were reduced (Figures 3H and 3I), indicating that DNA damage-activated p53 is required for hepatocyte death and liver injury. While apoptosis was drastically suppressed, inactivation of p53 significantly reduced survival and accelerated liver tumorigenesis (Figure 3J): 80% of mice displayed aggressive HCC (Figure 3K). Deletion of *Cdkn2a* did not modify mouse survival or tumor burden (data not shown). Thus, genotoxic stress, rather than excessive apoptosis, is the critical initiating event in liver carcinogenesis.

URI Causes DNA Damage and Liver Tumorigenesis by Inhibiting De Novo NAD+ Synthesis

To identify URI-mediated hepatocarcinogenetic events, we first examined mTOR activation, which had been implicated in HCC development via DNA damage (Menon et al., 2012). No increases in S6K1 activity were detected at 1 week (Figure S4A). In sequential immunoprecipitation experiments, using 1-week-old liver extracts, free hURI molecules were revealed by WB after complete depletion of PP1γ (Figures S4B and S4C), and vice versa (data not shown). When 3-week-old mice were supplied a rapamycin-containing diet, progression to preneoplastic abnormalities continued, if not further pronounced (data not shown). Thus, although a fraction of hURI binds PP1γ, hURI apparently has a PP1γ-independent role in DNA damage and liver tumorigenesis. Additionally, no differences in reactive oxygen species (ROS) were observed in 1- and 8-week-old livers (Figures S4D and S4E), suggesting that DNA damage is ROS-independent.

Global transcriptomic and proteomic profiling were performed in a very early nonpathological stage and early premalignant state (1- and 8-week-old livers). Transcripts' sequencing revealed small fractions of genes differentially expressed upon hURI expression: 303 out of 12,295 genes at 1 week, and 740 out of 11,133 (false discovery rate [FDR] < 0.05) at 8 weeks (Figures 4A and S4F). Similarly, isobaric tags for relative and absolute quantification (iTRAQ) identified 2,394 proteins: 122 and 597 of which were differentially expressed in 1- and 8-week livers, respectively (Figures 4B and S4G; Table S1).

Heatmapping revealed that most differentially expressed proteins were downregulated (Figure S4H). Significant overlaps in the differentially expressed transcripts and proteins at 1 and 8 weeks (Figures S4I and S4J), indicated hURI-dependent transcriptional repression mechanisms. Ingenuity pathway analysis (IPA) revealed that among canonical metabolic pathways, the L-tryptophan/kynurenine catabolism leading to de novo nicotinamide adenine dinucleotide (NAD^+) synthesis was one of the most significant downregulated pathways (Figures 4C and S4K). Enzymes implicated in the L-tryptophan/kynurenine degradation, including tryptophan 2,3-dioxygenase (TDO2) and arylformamidase (AFMID) catalyzing the initial rate-limiting step and kynurenine 3-monooxygenase (KMO), kynureninase (KNYU), and 3-hydroxyanthranilate 3,4-dioxygenase (HAAO) were all downregulated (Figure 4D). Gene set enrichment analysis (GSEA) (Subramanian et al., 2005), using the RNA sequencing data and Kyoto Encyclopedia of Genes and Genomes database, corroborated these defects (data not shown). WB confirmed that TDO2 and AFMID expression was reduced >50% in these livers (Figures 4E and S4L) and in adult livers expressing hURI (Figure S4M).

NAD^+ concentrations were reduced in 3- and 6-week mutant livers (Figures 4F and S4N), while increases in TDO2, AFMID, and NAD^+ levels were detected in $URI^{(+/\Delta)hep}$ livers (Figures 4G and 4H). Consistent with previous observations (Konishi et al., 1986), liver NAD^+ levels were depleted in DEN-treated mice, and URI reduction enhanced NAD^+ levels (Figure S4O). Thus, URI reduction enhances NAD^+ de novo synthesis, potentially explaining the protective effect of URI deletion in HCC. Furthermore, NAD^+ concentrations inversely correlated with URI levels in four human HCC cell lines (Huh-7, HepG2, SNU-398, and SNU-449). While URI depletion significantly increased NAD^+ levels, URI overexpression reduced NAD^+ values (Figure S4P). URI overexpression in SNU-449 cells, which had high NAD^+ values and low endogenous URI levels, increased their growth, whereas URI depletion in Huh-7 and HepG2 cells displaying high endogenous URI, significantly reduced their growth (Figure S4Q). URI-regulating NAD^+ levels may therefore be relevant for human liver tumorigenesis.

Depleting TDO2 and AFMID in HCC cell line SNU-449 significantly reduced NAD^+ levels (Figure S4R). Importantly, ^{14}C-labeled NAD^+ levels in four human HCC cell lines incubated with ^{14}C-tryptophan reduced significantly following AFMID depletion (Figure S4S), indicating that L-tryptophan degradation accounts for de novo NAD^+ synthesis. Furthermore, expression of key enzymes of three other pathways implicated in oncogenesis was unaffected by hURI expression: SHMT1, G6PD, and GOT1 of the glycine/serine/threonine, pentose phosphate and glutamine/aspartate pathways, respectively (Figure S4T). Finally, expression of nicotinamide phosphoribosyltransferase (NAMPT, implicated in NAD^+ biosynthesis through salvage reactions, Figure S4U) and activity of poly (ADP-ribose) polymerase (PARP), the main NAD^+-consuming enzyme (Figure S4U) were not affected at early stages (1 week), and levels of NADH and several dehydrogenases that reduce NAD^+ to NADH were decreased (Figure S4U; Table S2). Reduction of NAD^+ is thus mainly due to downregulation of L-tryptophan/kynurenine catabolism.

We next induced liver injury and hepatocyte proliferation in C57BL/6 mice with DDC-supplemented diet for 4 days, treated them with DMSO or Ro-61-8048, a KMO inhibitor, for the next 3 days, and sacrificed mice on day 8 (Figures S4V and S4W). NAD^+ concentrations were reduced and DNA damage foci significantly elevated in Ro-61-8048-treated livers (Figures 4I–4K). Thus, L-tryptophan/kynurenine pathway inhibition in vivo leads to reduced NAD^+ concentrations and DNA damage, recapitulating effects of hURI expression. Finally, nontumorigenic mouse liver cells AML-12, stably depleted of TDO2 and AFMID and transplanted into immunodeficient mice, formed aggressive tumors (Figure S4X), suggesting that inhibition of L-tryptophan pathway leads to transformation and tumorigenesis.

We assessed whether DNA damage was a consequence of inactivation of NAD^+-consuming enzymes, such as SIRT1 or PARP (Durkacz et al., 1980; Herranz et al., 2010). In SNU-449 cells, SIRT1 inhibition by EX-527, which may enhance NAD^+, reduced RPA32 phosphorylation, whereas activating SIRT1 with resveratrol, which may lower NAD^+, increased phosphorylation of RPA32 (Figure S4Y). Because in our model NAD^+ deficits increased replicative stress, DNA damage is unlikely due to SIRT1 inhibition alone. Additionally, in URI-overexpressing SNU-449 cells, in which NAD^+ levels were lowered (Figure S4P),

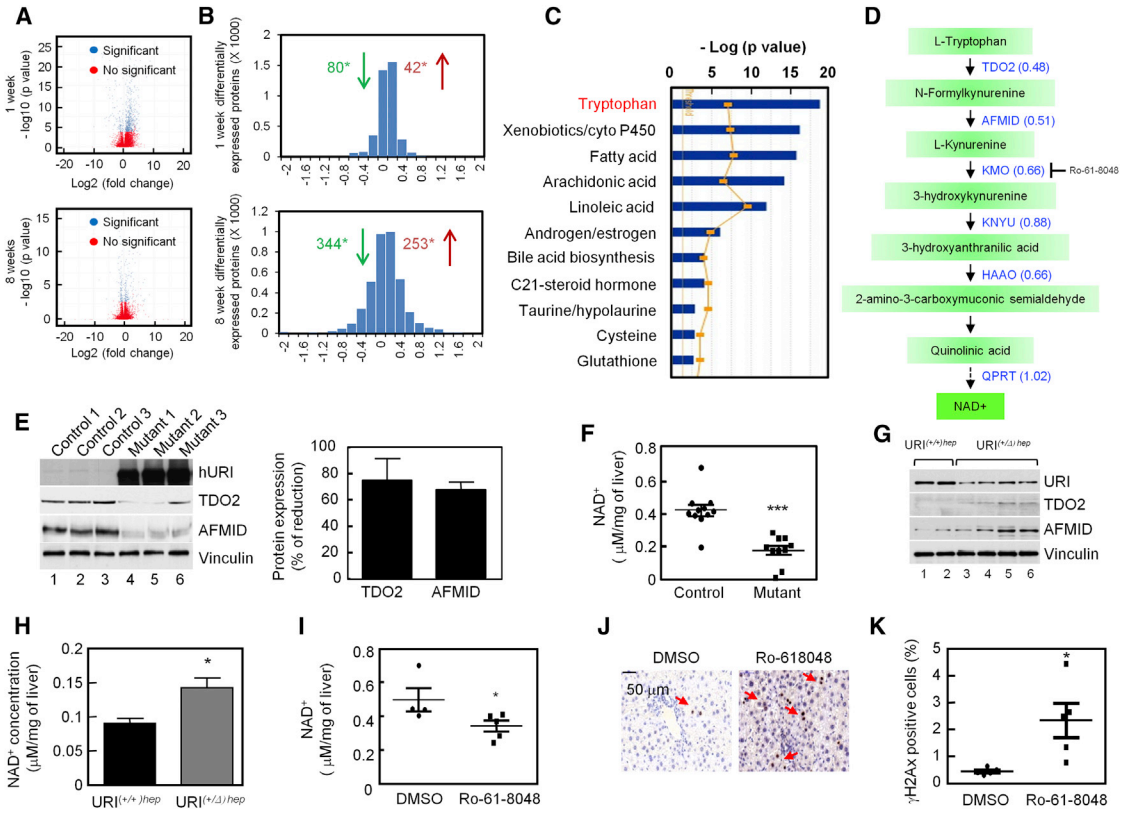

Figure 4. URI Causes DNA Damage and Liver Tumorigenesis by Inhibiting De Novo NAD+ Synthesis

(A) Volcano plots from RNA sequencing representing differentially expressed significant (blue) and unchanged (red) mRNA species in livers from 1- and 8-week-old hURI-tetOFF^{hep} mice. (n > 3).

(B) Histogram of differentially expressed proteins analyzed by iTRAQ in livers from 1- and 8-week-old hURI-tetOFF^{hep} mice. Numbers of proteins significantly downregulated (green) and upregulated (red) are shown. (n = 5).

(C) Top downregulated canonical metabolic pathways based on iTRAQ data from 8-week-old mice, analyzed by using IPA software.

(D) Scheme of de novo NAD+ synthesis. Fold change of protein expression detected in iTRAQ are represented within the brackets. Ro-61-8048 is an inhibitor for KMO.

(E) WB analysis (left) and quantification of reduction (mutant over control, right) of TDO2 and AFMID of 8-week-old hURI-tetOFF^{hep} livers.

(F) Liver NAD+ concentrations in 3-week-old hURI-tetOFF^{hep} mice. (n $\geq$ 10).

(G) WB analysis of URI$^{(+/+)hep}$ and URI$^{(+/\Delta)hep}$ livers.

(H) NAD+ levels in livers from URI$^{(+/+)hep}$ and URI$^{(+/\Delta)hep}$ mice. (n = 5).

(I) Liver NAD+ levels in C57BL/6 mice previously fed with DDC and treated with either DMSO (1%) or Ro-61-8048 (25 mg/Kg) compound. (n $\geq$ 5).

(J) Representative images of γH2AX IHC stained liver sections from C57BL/6 mice described in (I). (n = 5).

(K) Quantification of (J).

Data represented as mean ± SEM (*p $\leq$ 0.05 and ***p $\leq$ 0.001). See also Figure S4 and Tables S1 and S2.

SIRT1 activation further increased RPA32 phosphorylation. Thus, modulating SIRT1 activity may affect PARP activity either via modulation of NAD+ levels or through regulation of acetylation-dependent PARP1 activity (Rajamohan et al., 2009). Notably, URI overexpression increased RPA32 phosphorylation, which was not further enhanced when PARP was inhibited (Figure S4Y). Finally, PARP activity was reduced in 3-week-old mutants, while NAMPT expression remained unchanged (Figure S4Z). Thus, hURI-mediated NAD+ depletion may induce DNA damage via PARP inhibition.

Restoring NAD+ Pools Protects from DNA Damage and Prevents Tumor Formation

To investigate whether restoring NAD+ pools would prevent dysplastic nodules and tumor formation, 3-week-old hURI-tetOFF^{hep} mice were supplied with a nicotinamide riboside (NR) diet. NR significantly increased hepatic NAD+ concentrations (Figure S5A) without affecting liver-to-body weight ratio (Figure S5B). We detected dysplastic lesions and DNA damage in all mutants on chow, but not in those on NR, which also had reduced fibrosis, p53 abundance, and Ser-18 phosphorylation (Figures 5A–5D, S5C, and S5D). Prolonged NR treatment prevented tumor development and reduced ALT levels (Figures 5E–5G). Similarly liver tumors were prevented in 30-week-old homozygous mutants with higher URI levels (Figure S5E). Thus, restoring NAD+ pools protects from hURI-induced DNA damage, preneoplastic lesions, and tumor development. Surprisingly, 12-week-old homozygous mutants with full blown tumors then on 48 weeks of NR regimen showed significant tumor regression (Figures S5F and S5G), and their livers had high levels

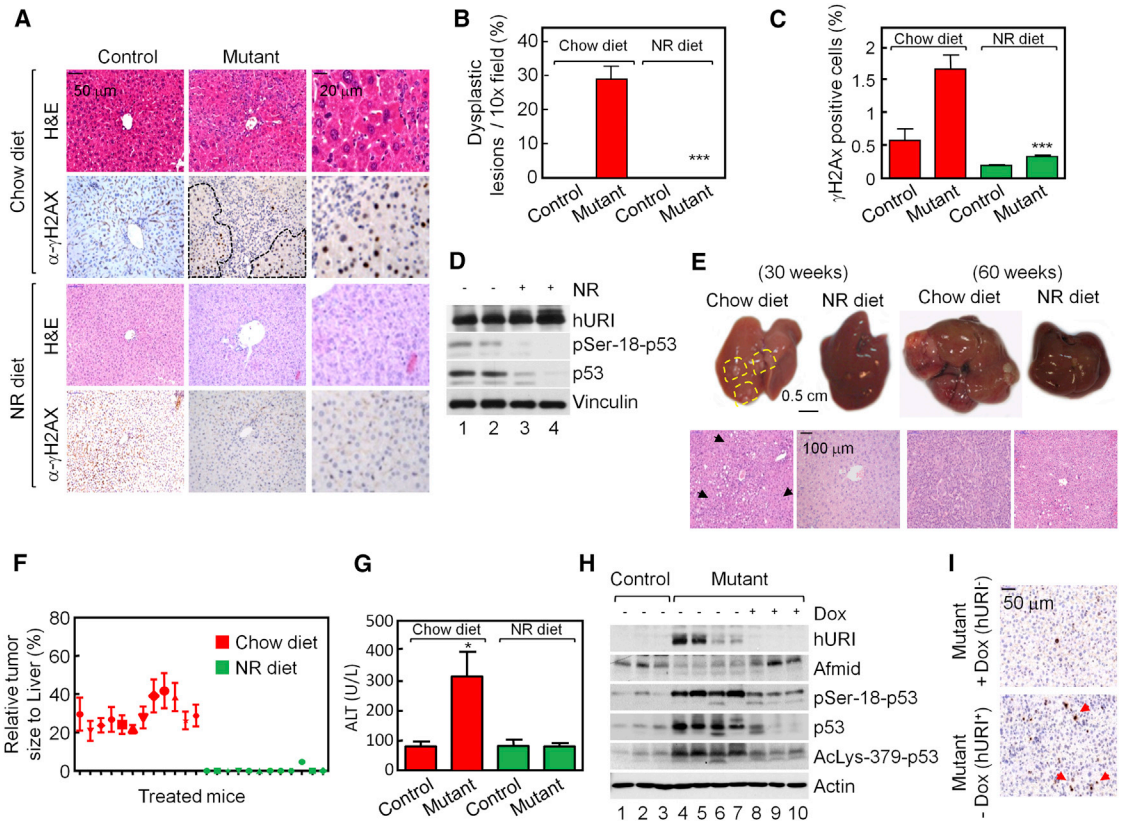

Figure 5. Restoring NAD+ Pools Protects from DNA Damage and Prevents Tumor Formation

(A) Representative images of H&E and γH2AX IHC stained liver sections from 12-week-old hURI-tetOFF^{hep} mice fed with either chow (n ≥ 15) or NR diets started at 3 weeks of age (n ≥ 15). Dotted black lines indicate anisokaryotic clusters present in mutant hURI-tetOFF^{hep} mice under chow diet.

(B) Quantification of dysplastic lesions in the hURI-tetOFF^{hep} mice described in (A).

(C) Quantification of γH2AX positive nuclei in the hURI-tetOFF^{hep} mice described in (A).

(D) WB analysis of mutant hURI-tetOFF^{hep} livers as described in (A).

(E) Representative images of whole livers and H&E stained liver sections from 30- or 60-week-old hURI-tetOFF^{hep} mice supplemented with NR diet from 3 weeks of age until mice were sacrificed. (n ≥ 10 for chow fed or NR fed.) Yellow dotted circles depict early tumors and black arrows point mitotic bodies.

(F) Tumor burden of 60-week-old mice described in (E).

(G) Serum ALT levels of 60-week-old mice described in (E).

(H) WB analysis of hURI-tetOFF^{hep} mice expressing hURI for 8 weeks and switched OFF for 24 weeks.

(I) γH2AX IHC stained liver sections from 32-week-old mutant hURI-tetOFF^{hep} mice fed with either chow or Dox diets. (n = 5). Red arrows point to DNA damage foci.

Data represented as mean ± SEM (*p ≤ 0.05 and ***p ≤ 0.001). See also Figure S5.

of cleaved caspase 3 (Figure S5H), suggesting that boosting NAD+ levels may be cytotoxic for tumor cells.

Furthermore, ceasing hURI expression in 8-week-old mice for 24 weeks restored AFMID levels, suppressed DNA damage, abolished the DDR, and reduced acetylation of p53 at Lys-379, possibly due to activated NAD+-dependent SIRT1 (Luo et al., 2001) (Figures 5H and 5I). Thus, continuous hURI expression and consequent inhibition of de novo NAD+ synthesis is essential for abolishing DNA repair and accelerating tumor formation.

Next, we explored whether other oncogenes had similar effects. *Ela-1-myc* mice, unlike K-*Ras*^{G12V} mice, develop pancreatic adenocarcinomas with high levels of DNA damage, while pancreatic tumors initiated by K-*Ras*^{G12V} show no signs of replicative stress (Murga et al., 2011). In early stages of tumorigenesis, c-Myc, but not K-RAS^{G12V}, expression induced DNA damage (Figures S5I and S5J). TOD2 and AFMID were clearly downregulated in *Ela-1-myc*, but not in K-*Ras*^{G12V} pancreas (Figure S5K). In 3-week-old *Ela-1-myc* mice, 4 weeks of NR diet did not affect acinar-to-ductal metaplasia (ADM), but 12 weeks of NR diet decreased ADM and carcinomas formation compared to chow fed mice (Figures S5L–S5O). Importantly pancreatic NAD+ levels were significantly reduced in *Ela-1-myc* mutants on chow diet, but restored to almost control levels on NR diet (Figure S5P). Thus, oncogene-induced DNA damage has a common bearing on NAD+ levels.

URI Regulates Kynurenine Metabolism by Modulating AhR and ER Activity

We found significant overlaps in differentially expressed transcripts between our RNA sequencing and published microarray data sets for livers from aryl hydrocarbon receptor (AhR) and estrogen receptor (ER) knockout mice (Figures 6A, S6A, and S6B), suggesting that AhR and ER mediate hURI-induced transcriptional repression of L-tryptophan/kynurenine catabolism. TDO2

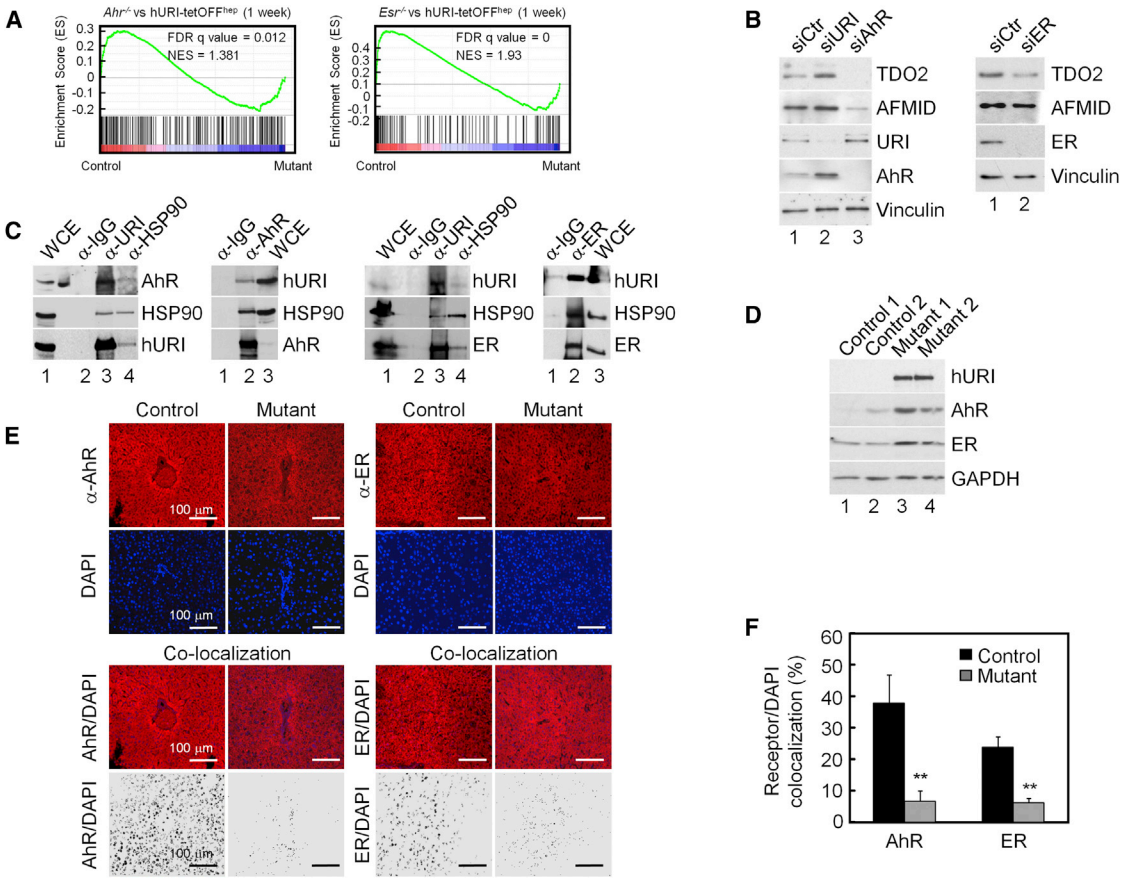

Figure 6. URI Regulates Kynurenine Metabolism by Modulating AhR and ER Activity

(A) GSEA using microarray data from *Ahr*$^{-/-}$ and *Esr*$^{-/-}$ livers and RNA sequencing data from 1 week hURI-tetOFF^{hep} mice.

(B) WB analysis of human HepG2 cells transfected with scramble (siCtr) or siRNA against URI (siURI), AhR (siAhR), or ER (siER).

(C) Immunoprecipitation of cytosolic liver fractions from 1 week hURI-tetOFF^{hep} mice and WB analysis.

(D) WB analysis of cytosolic fractions in livers from 1 week hURI-tetOFF^{hep} mice.

(E) AhR and ER immunofluorescence of 1 week hURI-tetOFF^{hep} liver sections. DAPI was used for nuclear staining. Lower panels depict nuclear colocalization performed by using Image J. (n = 5).

(F) Quantification of nuclear colocalization of AhR and ER shown in (E).

Data represented as mean ± SD (**p $\leq$ 0.01). See also Figure S6.

was also found deregulated in the core enriched *Esr*$^{-/-}$ data sets in GSEA analysis. Depletion of AhR and ER in HepG2 cells reduced expression of TDO2 (and AFMID), while URI downregulation increased their abundance (Figure 6B). ALGGEN-PROMO v3.0 software predicted several AhR and ER binding sites in genomic sequences 5 kilobases upstream of the transcriptional start sites of *TDO2* and *AFMID*. Chromatin immunoprecipitation assays revealed that both AhR and ER bound to these promoters in SNU-449 cells (Figures S6C and S6D). We also verified hURI-induced downregulation of other AhR and ER targets detected in the RNA sequencing and iTRAQ analyses, including carbomyl-phosphate synthase 1, glutayl-CoA dehydrogenase, and glycine N-methyltransferase 1 (GNMT1) (Figures S6E and S6F). Notably, *Gnmt1*$^{-/-}$ mice develop chronic hepatitis and spontaneous HCC (Liao et al., 2009). Thus, hURI can repress AhR and ER transcriptional activity, implicated in transcription of several metabolic enzymes in particular from the L-tryptophan catabolism pathway.

AhR and ER are in an inactive cytoplasmic complex with HSP90, a member of the URI prefoldin complex (Boulon et al., 2010; Knoblauch and Garabedian, 1999; Perdew, 1988). Reciprocal coimmunoprecipitation experiments confirmed that hURI and HSP90 interact with AhR or ER in cytosolic extracts of 1-week-old mutant livers (Figure 6C). Cytoplasmic fractions of mutant livers were also enriched with both nuclear receptors (Figure 6D). Immunofluorescence analysis detected significant reductions in nuclear AhR and ER in hepatocytes of 1-week-old mutants (Figures 6E, 6F, and S6G). Finally, nuclear and cytoplasmic fractionation of livers from 3-week-old DEN-treated URI$^{(+/+)hep}$ mice showed a positive correlation between URI expression and cytoplasmic AhR/ER localization, but an inverse correlation between nuclear URI and AhR/ER. In DEN-treated URI$^{(+/\Delta)hep}$ livers, AhR and ER were enriched in the nucleus (Figures S6H and S6I). Thus, hURI/HSP90 inhibitory cytoplasmic complex prevents AhR and ER transcriptional activity.

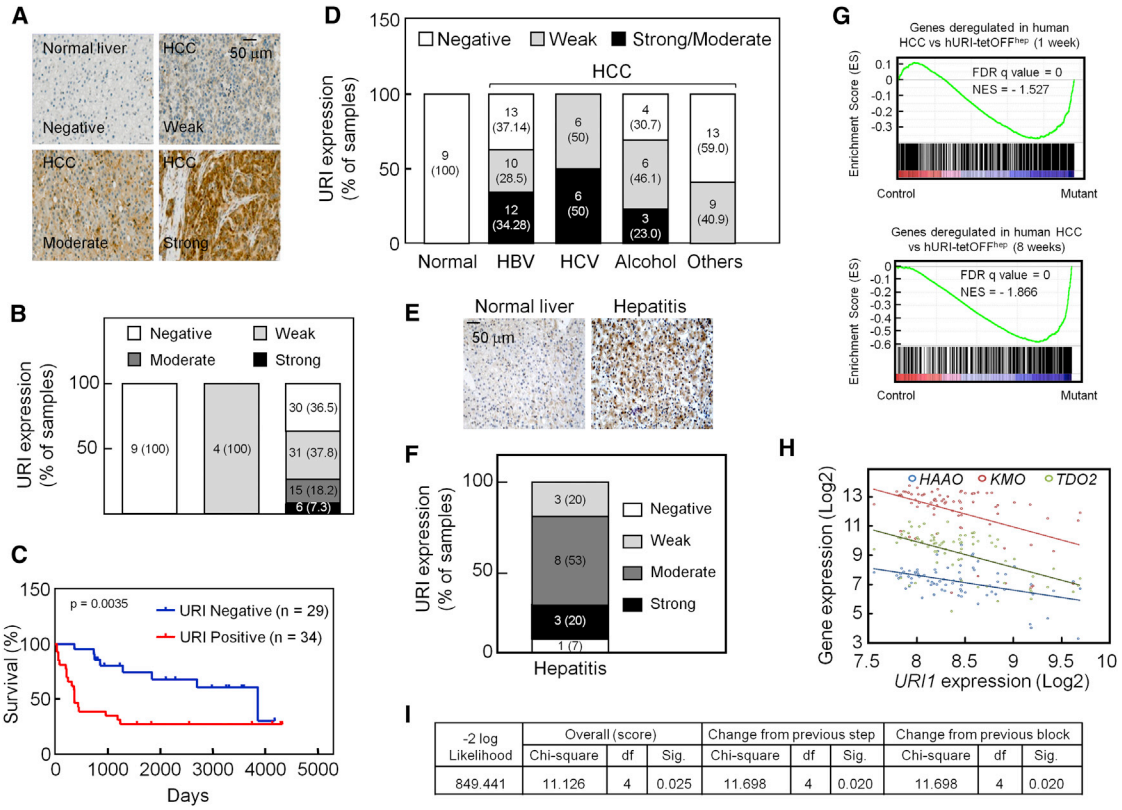

I

-2 log Likelihood	Overall (score)			Change from previous step			Change from previous block		
	Chi-square	df	Sig.	Chi-square	df	Sig.	Chi-square	df	Sig.
849.441	11.126	4	0.025	11.698	4	0.020	11.698	4	0.020

Figure 7. URI Expression Is Enhanced in HCC, Is Associated with Poor Survival, and Correlates with NAD+ Synthesis Inhibition

(A) Representative images of IHC stained for URI in human liver sections.

(B) Stratification of human samples according to URI expression as scored in (A). Values represent number of cases, and values within brackets represent percentage of total.

(C) Kaplan Meier analysis of overall patient survival based on IHC for URI expression in HCC. URI positive includes weak, moderate, and strong signal in IHC as described in (A). (Log rank test p = 0.0035; hazard ratio = 0.3163; and 95% confidence interval of ratio 0.1460 to 0.68).

(D) Stratification and correlation of URI expression in HCC samples with human HCC etiological factors.

(E) IHC for URI in normal and hepatitis human liver samples.

(F) Stratification of human hepatitis samples according to URI expression (n = 15). Values represent number of cases, and values within brackets represent percentage of total.

(G) GSEA between differentially expressed genes in human HBV-associated HCC and RNA sequencing data sets from 1- and 8-week-old hURI-tetOFF^{hep} mice.

(H) Linear regression analysis of *URI1* and *TDO2*, *KMO*, and *HAAO* expressions in a human HCC microarray data set, showing inverse correlation between *URI1* and *TDO2*, *KMO*, and *HAAO* expression.

(I) Multivariate Cox regression analysis for *TDO2*, *KMO*, *HAAO*, and *QPRT*, in a cohort of 221 HCC patients. (p = 0.025). "df" represents degrees of freedom and "Sig." represents significance. See also Figure S7.

URI Expression Is Enhanced in Human HCC, Is Associated with Poor Survival, and Correlates with De Novo NAD+ Synthesis Inhibition

We examined URI in a tissue-microarray (TMA) of human liver samples (82 HCC, 4 peritumoral, and 9 normal livers), using a specific URI antibody (Figure S7A). No URI was detected in normal livers, whereas various levels of URI were detected in HCC (Figures 7A and 7B). Increased URI levels in 20 human HCC, relative to paired peritumoral samples, were also detected by real-time PCR (data not shown) and WB. URI was approximately 2-fold higher in 70% of the tumoral tissues as in the peritumoral counterparts (Figures S7B and S7C), similar to hURI expression in the hURI-tetOFF^{hep} mouse. URI expression and Ki67 staining were positively correlated (Figure S7D). Importantly, URI expression was associated with poor prognosis (Figure 7C).

Data stratification indicated a significant correlation between URI and hepatitis B virus (HBV)- or hepatitis C virus (HCV)-associated HCC (Figure 7D). Increased URI expression was also observed in human hepatitis samples, which predisposes to hepatocarcinogenesis (Figures 7E and 7F). URI expression was thus analyzed in a concanavalin A (ConA)-induced mouse hepatitis model. C57BL/6 mice administered with ConA had a dramatic increase in hepatic URI after 4 to 8 hr. IHC analysis confirmed that URI was confined to hepatocytes (Figures S7E and S7F). Furthermore, HCC cell lines transiently transfected with HBV viral protein HBx enhanced URI expression (Figures S7G and S7H). When introduced into Huh-7 cells, expression of a mouse *Uri1* promoter luciferase reporter was increased about 1.5-fold by HBx (Figures S7I and S7J). Finally, GSEA detected significant overlaps between transcriptomic signatures

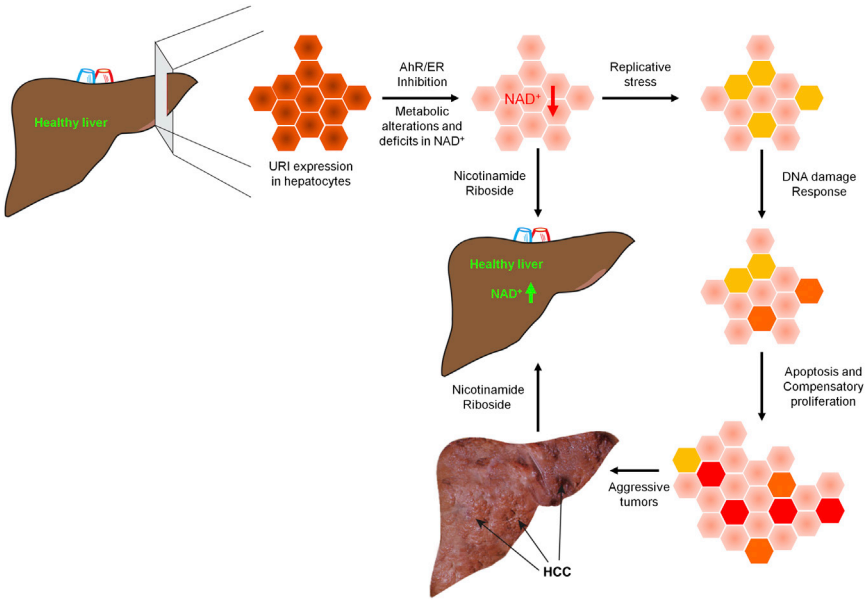

Figure 8. Scheme of URI-Induced HCC

Scheme representing molecular and cellular events of hepatocarcinogenesis induced by URI specifically expressed in hepatocytes. Hexagons represent hepatocytes.

of hURI genetically engineered mouse model (GEMM) and HBV-associated human HCC (Figure 7G). Thus, in human HCC, URI expression can be regulated by HBV infection or by infection-induced inflammatory cues.

Next, we examined correlations between URI and L-tryptophan/kynurenine pathway. WB analysis of the paired peritumoral/HCC samples revealed that AFMID and NAD+ levels were positively correlated, and both negatively correlated with URI expression (Figures S7K–S7O). Analysis of a human HCC gene expression data set (Wurmbach et al., 2007) showed inverse correlations between URI and TDO2, KMO and HAAO (Figure 7H). Finally, in a 221 patient data set (Roessler et al., 2010) (Gene Expression Omnibus [GEO] ID: GSE14520), Cox regression analysis of *TDO2*, *KMO*, *HAOO*, and quinolinate phosphoribosyltransferase (*QPRT*) expression, indicated that overall, patients' survival was significantly associated with L-tryptophan catabolism signature (Figures 7I and S7P). Downregulation of *TDO2* or *HAAO* also correlated with poor prognosis for HCC patients (Figures S7Q and S7R).

DISCUSSION

The presence of fibrosis/cirrhosis associated with chromosomal abnormalities is the most convincing clinical aspect of HCC, but the molecular mechanisms and pathogenesis of HCC are still poorly understood (Teoh et al., 2008). Using GEMMs, URI-mediated NAD+ depletion is shown to induce DNA damage, liver injury, and multistep HCC (Figure 8).

Liver injury predisposes to HCC (Malhi and Gores, 2008), but in our model ALT values at precancerous stages are normal. Normal ALT levels are observed in chronic HBV or HCV infected patients with mild to moderate histological liver damage (Nunnari et al., 2013), indicating that ALT levels are not always determinants for hepatic injuries. However, persistently elevated ALT increase HCC risks and are clear indicators of HCC in patients with viral hepatitis (Chen et al., 2011; Lee et al., 2010), suggesting that chronic hepatocyte death is a key trigger of liver disease progression (Luedde et al., 2014). Genotoxic stress-induced p53 is required for apoptosis, but when p53 is inactivated and hepatocyte death is reduced, carcinogenesis is accelerated. Thus, genotoxic stress via NAD+ deficits, rather than high-grade apoptosis, initiates liver tumorigenesis.

Therapies increasing NAD+ levels (e.g., NR) can be used to prevent HCC and cancers resulting from oncogene-induced DNA damage, but it remains to be determined whether boosting NAD+ is also therapeutic in nongenotoxic cancers. NR has also surprising therapeutic effects on fully developed liver tumors. Given that DNA damage-mediated chromosomal rearrangements are irreversible, boosting NAD+ levels may activate the mitochondria SIRT3, a proapoptotic tumor suppressor (Verma et al., 2013) enhancing cancer cell apoptosis and tumor regression. Elevated SIRT3 levels, specifically in tumor cells responding to NAD+ boost, remain to be elucidated.

Multiple epidemiologic studies report on the association between tryptophan-poor diets and increased specific cancer types incidences (Surjana et al., 2010). Daily supplementation of niacin, a NAD+ precursor, reduced esophageal cancer incidence and mortality in a population with chronic nutritional deficiency (Surjana et al., 2010), and, in which gut microbiota might be altered. Gut bacteria cleave the side chain of tryptophan (Burns and Demoss, 1962), limiting its concentration and use in de novo NAD+ synthesis (Michael et al., 1964). The implication of the intestinal microbiota was suggested in HCC development, although NAD+ levels remain to be determined (Dapito et al., 2012). Dysbiosis can also have a tumor promoting effect (Schwabe and Jobin, 2013), and malnutrition altering the intestinal flora induces HCC (Yoshimoto et al., 2013). Future cartographic determination of patients' microbiota and identification of specific harmful bacteria in diseases would be important to better understand the symbiosis between bacteria and mammals.

Activating AhR or ER can also be beneficial in HCC. Inhibiting AhR generates xenobiotic stress, which accelerates liver tumorigenesis (Walisser et al., 2005), and DEN-treated $AhR^{-/-}$ mice increased tumor incidence compared to their littermates, suggesting that AhR may be tumor suppressive (Fan et al., 2010). Several epidemiologic and animal studies also suggest a protective effect of estrogen (Naugler et al., 2007). Additionally, estrogen was effective in the treatment of traumatic liver injury (Hsieh et al., 2007). The nongender disparity in HCC development in our hURI mouse model is consistent with the role of ER inhibition in HCC progression.

URI inhibition may thus represent a therapeutic option at early stages of liver tumorigenesis, and combined therapies that synergistically activate AhR and ER should be tested in preclinical models for HCC treatment, in particular in patients with high URI expression. Finally, the development of more efficient and stable NAD^+ boosters could provide therapies to prevent or cure cancers and associated metabolic dysfunctions.

EXPERIMENTAL PROCEDURES

Generation and Handling of Mice

All mice have been backcrossed to C57BL/6 for at least seven generations and housed in pathogen-free conditions. All experiments were approved by the Centro Nacional de Investigaciones Oncologicas (CNIO)-Instituto de Salud Carlos III Ethics Committee and performed in accordance with the guidelines for ethical conduct in the care and use of animals as stated in the international guiding principles for biomedical research involving animals, developed by the Council for International Organizations of Medical Sciences. Littermates were always used as controls.

Liver Carcinogenesis, Injury Models, and Mouse Treatments

Fourteen-day-old mice were injected intraperitoneally with 25 mg/kg of DEN (Sigma) (Vesselinovitch and Mihailovich, 1983).

For ConA treatment, 8-week-old C57/BL6 male mice were intravenously injected with 15 mg/kg of ConA (Sigma Aldrich) and sacrificed at 2 hr intervals. DDC was mixed with chow diet to a final concentration of 0.5% w/w (Harlan) and supplied as indicated in the experiment.

Ro-61-8048 (Sigma-Aldrich, SML0233) was dissolved to 593 mM in DMSO. The 9-week-old C57BL/6 mice were given DDC for 4 days and then switched to chow and injected with either Ro-61-8048/Sunflower Seed Oil (25 mg/Kg) or DMSO/Sunflower Seed Oil (1:100) intraperitoneally for three consecutive days.

Nicotinamide riboside (97% purity, Waterstonetech Pharma) was dissolved in ice cold water and immediately mixed thoroughly with cold amorphous chow diet (Harlan) at 500 mg/kg/day and supplied ad-libitum.

Tumor Quantification

Macroscopically visible tumor nodules were counted and sizes measured with Vernier calipers. Total liver size was measured in the same position, and relative tumor burden was expressed as percentage of tumor volume relative to the whole liver.

Human Samples

Human samples were obtained from the histopathology files of University College Hospital, University College London (UCL), from patients after approval by the Institutional Research Ethics Committee (Central London REC 3, Reference 06/Q0512/106) and from the CNIO-Biobank. The construction and analysis of a tissue microarray of HCC was approved by the appropriate ethics committee, and informed consent was obtained from all subjects.

[^{14}C]-Tryptophan Metabolic Tracing

HCC cells were transfected with siCtr or siAFMID grown in a 12 well plate until they reached 60% confluence and starved for 5 hr for tryptophan in tryptophan-free media. 2.5 mM of [*benzene-ring-U*-^{14}C]-tryptophan was provided to cells and incubated at 37°C for 5 hr. Cells were then washed three times with cold PBS, and metabolites extracted in a methanol and water (80:20) mixture and incubated for 10 min at 4°C. Metabolic lysates were centrifuged at maximum speed for 20 min at 4°C. Radiolabeled samples were separated by thin layer chromatography (TLC) using ammonium acetate (1M, pH5) and ethanol (30:70) and cellulose F plates. Labeled NAD^+-[carbonyl-^{14}C] was used as positive control to calibrate the relative migration of labeled metabolites. TLC plates were dried and exposed to a PhosphorImager.

Proteomic Analysis

Extracted liver proteins were digested using a modified filter aided sample prep protocol. Peptides were labeled with iTRAQ reagents and samples were pooled. The complex mixture was subjected to isoelectric focusing fractionation. The resulting fractions were separated by on-line nano-liquid chromatography and analyzed by electrospray mass spectrometry (MS)/MS using a linear trap quadrupole Orbitrap Velos mass spectrometer (Thermo Scientific). Raw files were searched against UniProtKB/Swiss-Prot mouse database (release date, October 19, 2011; 16,407 entries) using MASCOT (Matrix Science, 2013). Peptides were filtered at 1% FDR using a concatenated database (see also Supplemental Experimental Procedures).

Reporter Assays

Evolutionarily conserved, 440 base pairs regulatory sequence of *URI* ORF were cloned in pGL4.10-Luc vector to generate the URI reporter plasmid. Huh-7 cells were transfected with 200 ng URI reporter and 5 ng Renilla encoding plasmids using Lipofectamine 2000. After 2 days of transfection, cells were analyzed using the Dual-Luciferase Reporter Assay System (#E1960, Promega). Values after pCDNA3-GFP or pCDNA3-HA-HBx transfection were normalized to a Renilla control.

Statistical Analyses

Statistical analyses were performed using GraphPad Prism V5.0 software (GraphPad Software, 2007). Statistical significance (p) ($p \leq 0.05$ = *, $p \leq 0.01$ = **, $p \leq 0.001$ = ***, and $p \leq 0.0001$ = ****) between the means of a minimum of three groups was determined using unpaired two-tailed Student's t test. Results are expressed as the mean value ± SD or ± SEM as indicated. All results including WB analysis are representative of at least three independent experiments. The Kaplan-Meier method was used to estimate survival curves for mouse and human, and log rank was used to evaluate statistical differences. Statistical parameter (FDR) estimates the probability of a gene set with false positive finding. Normalized enrichment score allows comparison of enrichment analysis results across gene sets. Cox regression and survival analysis were performed for target genes in human HCC data sets, using SPSS software (v20) (IBM, 2011).

ACCESSION NUMBERS

The proteomic data are deposited to the ProteomeXchange Consortium (http://proteomecentral.proteomexchange.org) via the PRIDE partner repository with the data set identifier PXD000296 (Vizcaino et al., 2013). RNA sequencing data are available from GEO (http://www.ncbi.nlm.nih.gov/geo) with the accession number GSE48654.

SUPPLEMENTAL INFORMATION

Supplemental Information includes Supplemental Experimental Procedures, seven figures, and two tables and can be found with this article online at http://dx.doi.org/10.1016/j.ccell.2014.10.002.

AUTHOR CONTRIBUTIONS

K.S.T. designed and performed most of the experiments. K.S.T. and N.D. engineered the ColhURI allele and generated the hURI-tetOFFhep mouse. A.L.G. analyzed fibrosis data. M.Y. and N.D. engineered the URI(lox/lox) allele and analyzed the URI promoter. O.G. and D.G.P. performed the bioinformatic analysis. L.B. and E.W. helped in generating the ColhURI allele. I.R. and P.X.E. performed the iTRAQ experiment. V.S. and M.R.J. analyzed the human liver samples. K.S.T. and N.D. analyzed all the data. N.D. designed the experiments and conceived, developed, and wrote the project and the manuscript. Funding was secured by N.D.

ACKNOWLEDGMENTS

We are thankful to F. Real and M. Barbacid for providing the *Ela-1-myc* and K-*Ras*^{G12V} pancreatic models, respectively. We thank R. Ricci, M. Serrano, R. Hamacher, G. Gomes, S. Wurm, F. Diaz, and S. Anderson for support and advice. K.S.T. is a recipient of La Caixa predoctoral fellowship. A.L.G. is a recipient of the Caja Navarra postdoctoral fellowship. P.X.E. is a recipient of the Fondo de Investigaciones Sanitarias grant (CA10/01231). M.R.J. is supported by UCL Hospitals Biomedical Research Centre. The E.F.W. lab is

supported by F-BBVA, the Spanish Ministry of Economy and Competitiveness (BFU201240230) and the European Research Council (ERC)-Advanced grant (ERC-FCK/2008/37). N.D. is a recipient of the Spanish Ramón y Cajal fellowship. This work was supported by the Spanish Ministry of Economy and Competitiveness (SAF2010 - 18518), the Association for International Cancer Research AICR-UK (11-0242), CNIO (BC1104-08), and the European Foundation for the Study of Diabetes.

Received: March 22, 2014
Revised: July 23, 2014
Accepted: October 2, 2014
Published: November 20, 2014

REFERENCES

Boulon, S., Pradet-Balade, B., Verheggen, C., Molle, D., Boireau, S., Georgieva, M., Azzag, K., Robert, M.C., Ahmad, Y., Neel, H., et al. (2010). HSP90 and its R2TP/Prefoldin-like cochaperone are involved in the cytoplasmic assembly of RNA polymerase II. Mol. Cell *39*, 912–924.

Burns, R.O., and Demoss, R.D. (1962). Properties of tryptophanase from Escherichia coli. Biochim. Biophys. Acta. *65*, 233–244.

Carpenter, B., Lin, Y., Stoll, S., Raffai, R.L., McCuskey, R., and Wang, R. (2005). VEGF is crucial for the hepatic vascular development required for lipoprotein uptake. Development *132*, 3293–3303.

Chen, C.F., Lee, W.C., Yang, H.I., Chang, H.C., Jen, C.L., Iloeje, U.H., Su, J., Hsiao, C.K., Wang, L.Y., You, S.L., et al. (2011). Changes in serum levels of HBV DNA and alanine aminotransferase determine risk for hepatocellular carcinoma. Gastroenterology *141*, 1240–1248, 1248 e1241–1242.

Dapito, D.H., Mencin, A., Gwak, G.Y., Pradere, J.P., Jang, M.K., Mederacke, I., Caviglia, J.M., Khiabanian, H., Adeyemi, A., Bataller, R., et al. (2012). Promotion of hepatocellular carcinoma by the intestinal microbiota and TLR4. Cancer Cell *21*, 504–516.

Djouder, N., Metzler, S.C., Schmidt, A., Wirbelauer, C., Gstaiger, M., Aebersold, R., Hess, D., and Krek, W. (2007). S6K1-mediated disassembly of mitochondrial URI/PP1gamma complexes activates a negative feedback program that counters S6K1 survival signaling. Mol. Cell *28*, 28–40.

Durkacz, B.W., Omidiji, O., Gray, D.A., and Shall, S. (1980). (ADP-ribose)n participates in DNA excision repair. Nature *283*, 593–596.

El-Serag, H.B. (2011). Hepatocellular carcinoma. N. Engl. J. Med. *365*, 1118–1127.

Fan, Y., Boivin, G.P., Knudsen, E.S., Nebert, D.W., Xia, Y., and Puga, A. (2010). The aryl hydrocarbon receptor functions as a tumor suppressor of liver carcinogenesis. Cancer Res. *70*, 212–220.

Herranz, D., Muñoz-Martin, M., Cañamero, M., Mulero, F., Martinez-Pastor, B., Fernandez-Capetillo, O., and Serrano, M. (2010). Sirt1 improves healthy ageing and protects from metabolic syndrome-associated cancer. Nat. Commun. *1*, 3.

Hsieh, Y.C., Yu, H.P., Frink, M., Suzuki, T., Choudhry, M.A., Schwacha, M.G., and Chaudry, I.H. (2007). G protein-coupled receptor 30-dependent protein kinase A pathway is critical in nongenomic effects of estrogen in attenuating liver injury after trauma-hemorrhage. Am. J. Pathol. *170*, 1210–1218.

Ito, A., Lai, C.H., Zhao, X., Saito, S., Hamilton, M.H., Appella, E., and Yao, T.P. (2001). p300/CBP-mediated p53 acetylation is commonly induced by p53-activating agents and inhibited by MDM2. EMBO J. *20*, 1331–1340.

Kang, J.S., Wanibuchi, H., Morimura, K., Gonzalez, F.J., and Fukushima, S. (2007). Role of CYP2E1 in diethylnitrosamine-induced hepatocarcinogenesis in vivo. Cancer Res. *67*, 11141–11146.

Knoblauch, R., and Garabedian, M.J. (1999). Role for Hsp90-associated cochaperone p23 in estrogen receptor signal transduction. Mol. Cell. Biol. *19*, 3748–3759.

Konishi, Y., Takahashi, S., Nakae, D., Uchida, K., Tsutsumi, M., Shiraiwa, K., and Denda, A. (1986). Possible model of liver carcinogenesis using inhibitors of NAD+ ADP ribosyl transferase in rats. Toxicol. Pathol. *14*, 483–488.

Kudo, M. (2009). Multistep human hepatocarcinogenesis: correlation of imaging with pathology. J. Gastroenterol. *44* (*Suppl 19*), 112–118.

Lee, M.H., Yang, H.I., Lu, S.N., Jen, C.L., Yeh, S.H., Liu, C.J., Chen, P.J., You, S.L., Wang, L.Y., Chen, W.J., and Chen, C.J. (2010). Hepatitis C virus seromarkers and subsequent risk of hepatocellular carcinoma: long-term predictors from a community-based cohort study. J. Clin. Oncol. *28*, 4587–4593.

Liao, Y.J., Liu, S.P., Lee, C.M., Yen, C.H., Chuang, P.C., Chen, C.Y., Tsai, T.F., Huang, S.F., Lee, Y.H., and Chen, Y.M. (2009). Characterization of a glycine N-methyltransferase gene knockout mouse model for hepatocellular carcinoma: Implications of the gender disparity in liver cancer susceptibility. Int. J. Cancer *124*, 816–826.

Libbrecht, L., Craninx, M., Nevens, F., Desmet, V., and Roskams, T. (2001). Predictive value of liver cell dysplasia for development of hepatocellular carcinoma in patients with non-cirrhotic and cirrhotic chronic viral hepatitis. Histopathology *39*, 66–73.

Luedde, T., Kaplowitz, N., and Schwabe, R.F. (2014). Cell death and cell death responses in liver disease: Mechanisms and clinical relevance. Gastroenterology *147*, 765, e4.

Luo, J., Nikolaev, A.Y., Imai, S., Chen, D., Su, F., Shiloh, A., Guarente, L., and Gu, W. (2001). Negative control of p53 by Sir2alpha promotes cell survival under stress. Cell *107*, 137–148.

Malhi, H., and Gores, G.J. (2008). Cellular and molecular mechanisms of liver injury. Gastroenterology *134*, 1641–1654.

Menon, S., Yecies, J.L., Zhang, H.H., Howell, J.J., Nicholatos, J., Harputlugil, E., Bronson, R.T., Kwiatkowski, D.J., and Manning, B.D. (2012). Chronic activation of mTOR complex 1 is sufficient to cause hepatocellular carcinoma in mice. Sci. Signal. *5*, ra24.

Michael, A.F., Drummond, K.N., Doeden, D., Anderson, J.A., and Good, R.A. (1964). Tryptophan metabolism in man. J. Clin. Invest. *43*, 1730–1746.

Murga, M., Campaner, S., Lopez-Contreras, A.J., Toledo, L.I., Soria, R., Montaña, M.F., D'Artista, L., Schleker, T., Guerra, C., Garcia, E., et al. (2011). Exploiting oncogene-induced replicative stress for the selective killing of Myc-driven tumors. Nat. Struct. Mol. Biol. *18*, 1331–1335.

Naugler, W.E., Sakurai, T., Kim, S., Maeda, S., Kim, K., Elsharkawy, A.M., and Karin, M. (2007). Gender disparity in liver cancer due to sex differences in MyD88-dependent IL-6 production. Science *317*, 121–124.

Nunnari, G., Pinzone, M.R., and Cacopardo, B. (2013). Lack of clinical and histological progression of chronic hepatitis C in individuals with true persistently normal ALT: the result of a 17-year follow-up. J. Viral Hepat. *20*, e131–e137.

Perdew, G.H. (1988). Association of the Ah receptor with the 90-kDa heat shock protein. J. Biol. Chem. *263*, 13802–13805.

Pilati, C., Letouzé, E., Nault, J.C., Imbeaud, S., Boulai, A., Calderaro, J., Poussin, K., Franconi, A., Couchy, G., Morcrette, G., et al. (2014). Genomic profiling of hepatocellular adenomas reveals recurrent FRK-activating mutations and the mechanisms of malignant transformation. Cancer Cell *25*, 428–441.

Rajamohan, S.B., Pillai, V.B., Gupta, M., Sundaresan, N.R., Birukov, K.G., Samant, S., Hottiger, M.O., and Gupta, M.P. (2009). SIRT1 promotes cell survival under stress by deacetylation-dependent deactivation of poly(ADP-ribose) polymerase 1. Mol. Cell. Biol. *29*, 4116–4129.

Reinhardt, H.C., and Schumacher, B. (2012). The p53 network: cellular and systemic DNA damage responses in aging and cancer. Trends Genet. *28*, 128–136.

Roessler, S., Jia, H.L., Budhu, A., Forgues, M., Ye, Q.H., Lee, J.S., Thorgeirsson, S.S., Sun, Z., Tang, Z.Y., Qin, L.X., and Wang, X.W. (2010). A unique metastasis gene signature enables prediction of tumor relapse in early-stage hepatocellular carcinoma patients. Cancer Res. *70*, 10202–10212.

Schuler, M., Dierich, A., Chambon, P., and Metzger, D. (2004). Efficient temporally controlled targeted somatic mutagenesis in hepatocytes of the mouse. Genesis *39*, 167–172.

Schwabe, R.F., and Jobin, C. (2013). The microbiome and cancer. Nature Reviews *13*, 800–812.

Subramanian, A., Tamayo, P., Mootha, V.K., Mukherjee, S., Ebert, B.L., Gillette, M.A., Paulovich, A., Pomeroy, S.L., Golub, T.R., Lander, E.S., and

Mesirov, J.P. (2005). Gene set enrichment analysis: a knowledge-based approach for interpreting genome-wide expression profiles. Proc. Natl. Acad. Sci. USA *102*, 15545–15550.

Surjana, D., Halliday, G.M., and Damian, D.L. (2010). Role of nicotinamide in DNA damage, mutagenesis, and DNA repair. J. Nucleic Acids *2010*, 2010.

Teoh, N.C., Dan, Y.Y., Swisshelm, K., Lehman, S., Wright, J.H., Haque, J., Gu, Y., and Fausto, N. (2008). Defective DNA strand break repair causes chromosomal instability and accelerates liver carcinogenesis in mice. Hepatology *47*, 2078–2088.

Theurillat, J.P., Metzler, S.C., Henzi, N., Djouder, N., Helbling, M., Zimmermann, A.K., Jacob, F., Soltermann, A., Caduff, R., Heinzelmann-Schwarz, V., et al. (2011). URI is an oncogene amplified in ovarian cancer cells and is required for their survival. Cancer Cell *19*, 317–332.

Trinidad, A.G., Muller, P.A., Cuellar, J., Klejnot, M., Nobis, M., Valpuesta, J.M., and Vousden, K.H. (2013). Interaction of p53 with the CCT complex promotes protein folding and wild-type p53 activity. Mol. Cell *50*, 805–817.

Verma, M., Shulga, N., and Pastorino, J.G. (2013). Sirtuin-3 modulates Bak- and Bax-dependent apoptosis. J. Cell Sci. *126*, 274–288.

Vesselinovitch, S.D., and Mihailovich, N. (1983). Kinetics of diethylnitrosamine hepatocarcinogenesis in the infant mouse. Cancer Res. *43*, 4253–4259.

Vizcaino, J.A., Cote, R.G., Csordas, A., Dianes, J.A., Fabregat, A., Foster, J.M., Griss, J., Alpi, E., Birim, M., Contell, J., et al. (2013). The PRoteomics IDEntifications (PRIDE) database and associated tools: status in 2013. Nucleic Acids Res. *41*, D1063–D1069.

Walisser, J.A., Glover, E., Pande, K., Liss, A.L., and Bradfield, C.A. (2005). Aryl hydrocarbon receptor-dependent liver development and hepatotoxicity are mediated by different cell types. Proc. Natl. Acad. Sci. USA *102*, 17858–17863.

WHO. (2008). Tumours of the liver and intrahepatic bile ducts. In Pathology and Genetics of Tumors of the Digestive System, S.R. Hamilton and L.A. Aaltonen, eds. (IARC Press). http://www.iarc.fr/en/publications/pdfs-online/pat-gen/bb2/BB2.pdf.

Wurmbach, E., Chen, Y.B., Khitrov, G., Zhang, W., Roayaie, S., Schwartz, M., Fiel, I., Thung, S., Mazzaferro, V., Bruix, J., et al. (2007). Genome-wide molecular profiles of HCV-induced dysplasia and hepatocellular carcinoma. Hepatology *45*, 938–947.

Yoshimoto, S., Loo, T.M., Atarashi, K., Kanda, H., Sato, S., Oyadomari, S., Iwakura, Y., Oshima, K., Morita, H., Hattori, M., et al. (2013). Obesity-induced gut microbial metabolite promotes liver cancer through senescence secretome. Nature *499*, 97–101.